

# Feature extraction of particle density in a pipeline with tomography and wavelets

Masahiro Takei<sup>a,\*</sup>, Hui Li<sup>b</sup>, Mitsuaki Ochi<sup>a</sup>, Yoshifuru Saito<sup>c</sup> and Kiyoshi Horii<sup>d</sup>

<sup>a</sup>*Nihon University, Dept of Mech. Eng. 1-8-14 Kanda Surugadai Tokyo, Japan 101-8308*

<sup>b</sup>*Kagoshima University, Kagoshima Japan*

<sup>c</sup>*Hosei University, Tokyo, Japan*

<sup>d</sup>*Shirayuri College, Tokyo, Japan*

**Abstract.** A concept to extract a feature of solid-air two-phase flow in a pipeline has been launched with a combination of a capacitance-computed tomography and wavelets transform. With this concept, particle distribution images obtained by CT are transformed with discrete wavelets multiresolution. As a result, in the case of low open area ratios of the pipe cross-section, high particle densities are shown in secondary dominant levels as well as a substantial space level. The high value in the secondary level resulted from inhomogeneous density due to collision between particles.

## 1. Introduction

Air transportation of particle in a pipeline should evade choking phenomenon that the suspended particle plugs the pipeline. Our research group has been investigating the minimum transportation velocity [1], spiral flow transportation [2] and a specially shaped bend [3] to avoid the choking phenomenon. Recently, the authors have started investigating a monitoring method for the particle behavior with real time by using computed tomography (CT). In a field of air-liquid two-phase flow, a high speed X ray CT device that can continuously obtain two dimensional distribution at 0.5 ms interval has been developed [4]. However, the device is not suitable for general choking diagnosis industrially because X ray CT is very expensive, and needs a license for the operation. Recently, a capacitance CT with real time has been studied as a technique to visualize particle behavior in solid-air two-phase flow [5,6]. This capacitance CT arranges a sensor consisting of many electrodes around a pipeline circumference to measure the capacitances among electrodes. The particle distribution based on the permittivity on the cross section is obtained from a re-constitution. However, the images acquired by the CT are blurred because approximate values are resolved by mathematical ill-posed inverse problem. An image analysis is needed to extract the feature of the blurred image to judge the pipeline emergency. Currently, discrete wavelets transform [7] has been used for image analysis in engineering fields. The analysis enables us to decompose and to compose a image in an orthonormal space. The authors applied this idea to analyse of electromagnetic wave [8] and a jet image [9].

The originality of this paper lies in applying discrete wavelets transform to capacitance CT images as a first step to judge the pipeline emergency. In this study, capacitances of particles in a vertical pipeline that installs a blockage are measured to extract the feature image.

---

\*Corresponding author: Masahiro Takei, Fax: +81 3 3293 8254; E-mail: takei@mech.cst.nihon-u.ac.jp.

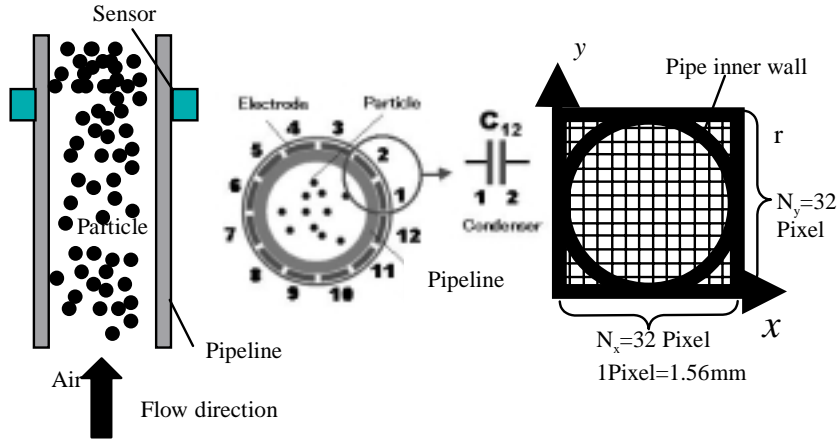


Fig. 1. (A) Front & Cross section views, (B) Space resolution Overview of capacitance tomography.

## 2. Experiments

### 2.1. Experimental equipment, condition and method

The capacitance CT device arranges a sensor at a pipeline circumference as shown in Fig.1 (A). Insulation materials separate the 12 electrodes in the sensor. The relation between capacitance and permittivity  $\varepsilon$  in electro-static field is expressed by

$$C_{i,j} = -\frac{\varepsilon_0}{V_c} \oint_{\mathbf{r} \in \Gamma_j} \varepsilon(\mathbf{r}) \nabla V_i(\mathbf{r}) \cdot d\mathbf{r}. \quad (1)$$

Where,  $i$  is a standard electrode which is from 1 to 11, and  $j$  is a reference electrode which is from  $i + 1$  to 12.  $C_{i,j}$  is the capacitance between the standard electrode  $i$  and the reference electrode  $j$ .  $\varepsilon_0$  is vacuum permittivity of air,  $\varepsilon(\mathbf{r})$  is permittivity distribution on the cross section which indicates the particle distribution.  $\mathbf{r}$  is a position vector on the cross section.  $V_c$  is a potential to the  $i$  electrode.  $V_i(\mathbf{r})$  is the potential distribution on the cross section between  $i$  and  $j$  electrodes. Because  $V_i(\mathbf{r})$  is unknown in Eq. (1), the following Laplace equation,

$$\nabla \cdot [\varepsilon(\mathbf{r}) \nabla V(\mathbf{r})] = 0 \quad (2)$$

is assumed on the cross section.  $V(\mathbf{r})$  is obtained by FEM from the discretized Eq. (2). The matrix expression of Eq. (1) showing the relation between the capacitance matrix  $\mathbf{C}$  and the permittivity distributions  $\mathbf{E}$  is

$$\mathbf{C} = \mathbf{S}_e \mathbf{E}. \quad (3)$$

Where, the sensitivity map matrix  $\mathbf{S}_e$  consists of the known values of  $\varepsilon_0$ ,  $V_c$  and  $\nabla V_i(\mathbf{r})$  in Eq. (1). In other words, the capacitance CT has a method to obtain the permittivity distribution of the particle  $\mathbf{E}$  on the cross section from both known sensitivity map matrix  $\mathbf{S}_e$  and the measured capacitance matrix  $\mathbf{C}$ . In the case that the pipeline cross section is divided with  $32 \times 32 = 1024$  square mesh as shown in Fig. 1(B) and the electrodes number is twelve, the sensitivity map  $\mathbf{S}_e$  is a  $66 \times 1024$  matrix in Eq. (3), the capacitance matrix  $\mathbf{C}$  expresses a  $66 \times 1$  matrix, and the permittivity distribution matrix  $\mathbf{E}$  is a  $1024 \times 1$

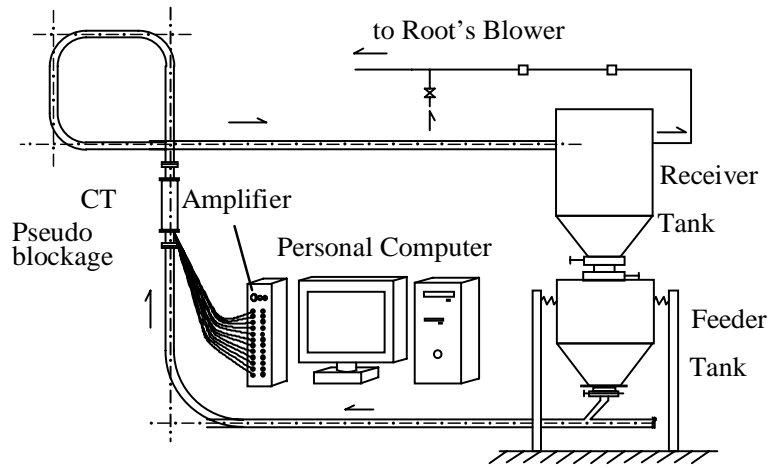






Fig. 2. Experimental equipment.

Table 1  
Experimental condition

Open area ratio $S$ [-]			
1.000	0.805	0.500	0.195
			 Blockage
Case1	Case2	Case3	Case4

matrix. The mathematical method to obtain the permittivity matrix  $\mathbf{E}$  from the capacitance matrix  $\mathbf{C}$  and the sensitivity map matrix  $\mathbf{S}e$  is an ill posed inverse problem. The image is reconstructed by a liner back projection method.

The experimental equipment is composed of a feeder tank, pipeline of 50.0 mm inside diameter, a receiver tank and a roots blower as shown in Fig. 2. The pipeline is composed of a 4.0 m long vertical pipe, bend pipes and horizontal pipes. A clay blockage is installed in the vertical pipe at 2.0 m point from the bottom to observe the particle behavior at the downstream of the blockage part. The air suction volume is 0.034 m<sup>3</sup>/s, the particle is supplied at 0.54 kg/s. The mean air velocity in the pipeline calculated from the air volume is 16.8 m/s, Reynolds number is  $4.71 \times 10^4$ , and the solid air ratio is 16.7. The blockage part has four type ratios of 0, 1/4, 1/2 and 3/4 of the pipe cross-section area as shown in Table 1. Therefore, the open area ratios  $S$  are 1.0, 0.805, 0.500 and 0.195. The conditions from Case1 to Case4 are set up as shown in Table 1. The particles are polyethylene pellets, which are almost spherical with 3.26 mm diameter and 910 kg/m<sup>3</sup> density. The CT acquires 100 frames every 1.0 s.

## 2.2. Experimental results

Each two dimensional particle distribution image  $\mathbf{E}_{xyt}$  for 50.0 ms is transformed to the density fluctuation distribution  $\mathbf{E}'_{xyt}$  using the mean value of the whole image and the mean square value  $\mathbf{E}_{RMS}$  of the whole image,

$$\mathbf{E}'_{xyt} = (\mathbf{E}_{xyt} - \bar{\mathbf{E}}) / \mathbf{E}_{RMS} \tag{4}$$

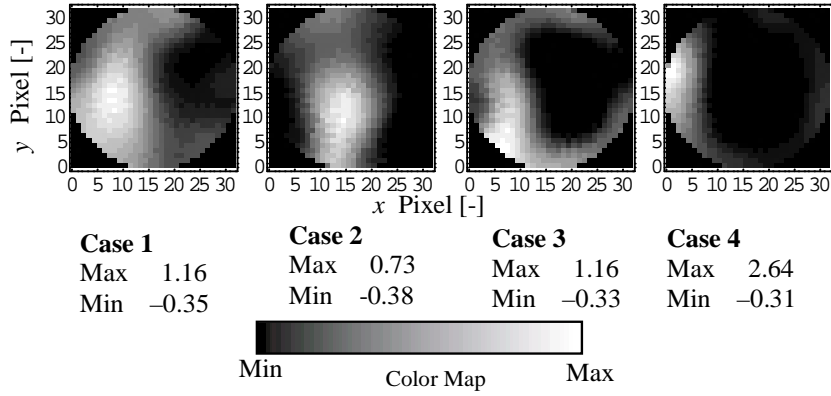


Fig. 3. Time mean particle density CT image.

Table 2  
Relation between wavelet level and representative space frequency

Level	Space frequency [mm <sup>-1</sup> ]	Space size [mm]	Mean value of space size [mm]
L0	0.02~0.05	50~20	35.0
L1	0.05~0.06	20~14.6	17.3
L2	0.06~0.11	14.6~9.2	11.9
L3	0.11~0.21	9.2~4.8	7.0
L4	0.21~0.32	4.8~3.1	3.95

$$\bar{\mathbf{E}} = \frac{1}{N_t N_y N_x} \sum_{t=1}^{N_t} \sum_{y=1}^{N_y} \sum_{x=1}^{N_x} \mathbf{E}_{xyt} \quad (5)$$

$$\mathbf{E}_{\text{RMS}} = \frac{1}{N_t N_y N_x} \sum_{t=1}^{N_t} \sum_{y=1}^{N_y} \sum_{x=1}^{N_x} \sqrt{(\mathbf{E}_{xyt} - \bar{\mathbf{E}})^2} \quad (6)$$

The particle density image  $\mathbf{E}'_{xyt}$  is changed to the time mean value,

$$\bar{\mathbf{E}}'_{xy} = \frac{1}{N_t} \sum_{t=1}^{N_t} \mathbf{E}'_{xyt} \quad (7)$$

Where,  $N_x$ ,  $N_y$  and  $N_t$  are the space resolution of  $x$  and  $y$  axes and the frame number in time as showed in Fig. 1(B). In this study,  $N_x = N_y = 32$  and  $N_t = 50$ . The time mean density images are shown in Fig. 3. The image elements, where any particle does not exist, are black. As the particle density on an image element becomes high, the image element changes into white with 10 stages in the color bar. On the whole, the particle distribution is qualitatively visualized at every condition. In the case of  $S = 1.0$  (Case1), the particles are distributed at relatively center position. However, the particle distribution gets partial as the open area ratios  $S$  decreases. In particular, the extremely partial particle distribution is visualized in  $S = 0.195$ .

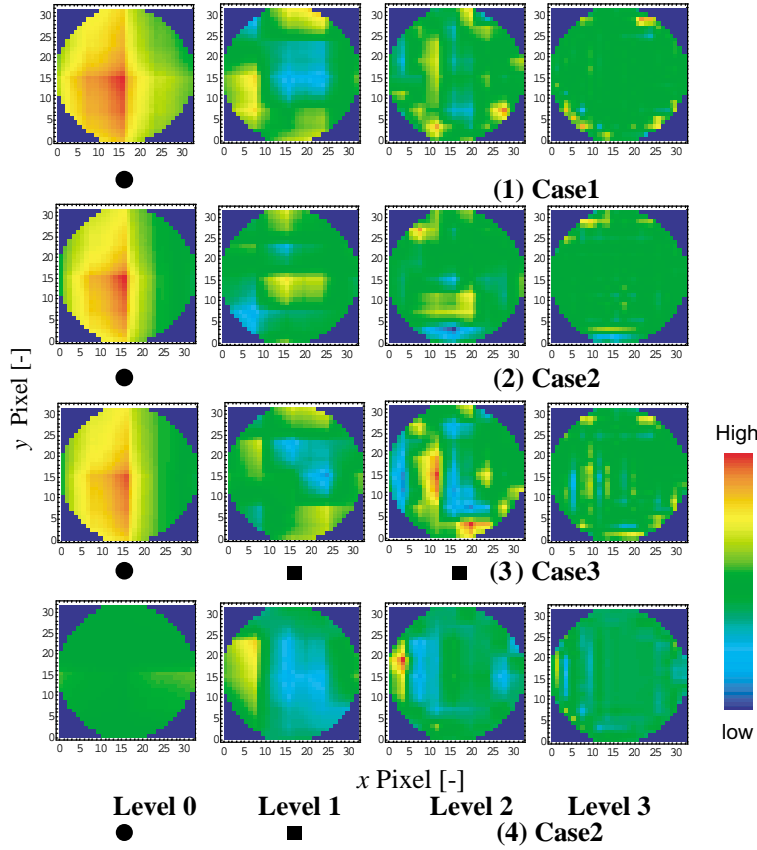


Fig. 4. Multiresolution of CT image.

### 3. Image processing and discussion

#### 3.1. Method and results

Two-dimensional wavelets transform of  $n \times n$  matrix  $\mathbf{E}$  is expressed by

$$\mathbf{S} = \mathbf{W}\mathbf{E}\mathbf{W}^T. \tag{8}$$

Where,  $\mathbf{W}$  is an analyzing wavelet matrix,  $\mathbf{W}^T$  is the transpose matrix of  $\mathbf{W}$  and  $\mathbf{S}$  is the spectrum. In the case of Daubechies function of fourth order and 32 X 32 image element data ( $n = 32$ ), the multiresolution classifies to four levels as shown in

$$\mathbf{E} = \mathbf{W}^T\mathbf{S}\mathbf{W} = \mathbf{W}^T\mathbf{S}_0\mathbf{W} + \mathbf{W}^T\mathbf{S}_1\mathbf{W} + \mathbf{W}^T\mathbf{S}_2\mathbf{W} + \mathbf{W}^T\mathbf{S}_3\mathbf{W} + \mathbf{W}^T\mathbf{S}_4\mathbf{W}. \tag{9}$$

$\mathbf{W}^T\mathbf{S}_0\mathbf{W}$  shows the lowest space frequency called Level 0.  $\mathbf{W}^T\mathbf{S}_4\mathbf{W}$  shows the highest space frequency called Level 4. The space frequency and the space size calculated by Fourier transform to the Daubechies function are shown in Table 2. Figure 4 shows the multiresolution of the time mean particle density images in Fig. 3. Each level shows a particle distribution with particle lump that has the specific space frequency in Table 2. The red shows the high particle density, and the blue is opposite. The levels in the

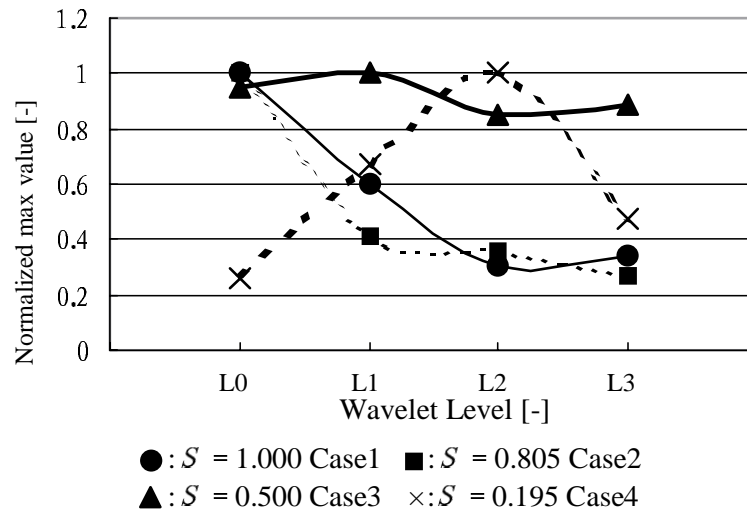


Fig. 5. Max values in wavelet multiresolution images.

same experimental case have the same color map. Addition from the level 0 to the level 4 (the level 4 is not shown) recovers Fig. 3 completely due to the orthonormal wavelet transform. In the case of  $S = 1.0$  (Case1) and 0.805 (Case2), a high value of the particle density is found in the level 0 to indicate a large particle lump (● symbol); however, a high value of the particle density is not found conspicuously in a higher level than the level 0. On the other hand, in the case of  $S = 0.5$  (Case3) and 0.195 (Case4), a high value of the particle density is found in the level 0 or the level 1 to indicate a large particle lump (● symbol); moreover, a high value is also found in a higher level than these low levels. Especially, Case 3 has the levels 1 and 2, and Case 4 has the level 2 (■ symbol). Therefore, when the open area ratio  $S$  is large, only a substantial space level which is equivalent to the open area indicates the high value; however, when the open area ratio  $S$  is small, a secondary dominant level exists in higher level as well as the substantial space level.

The maximum value of the multiresolution in Fig. 4 is quantitatively obtained in order to confirm the proper characteristic of the images. Fig. 5 shows the maximum value of the multiresolution image pixels as a parameter of the open area ratio  $S$ . When the open area ratio  $S$  is large (Cases 1 and 2), the maximum value decreases dramatically at the level 1 to maintain it low after the level. However, when the open area ratio  $S$  is a little small (Case 3), a high value is shown in every level. Moreover, when the open area ratio  $S$  is very small (Case 4), the minimum value in the level 0 increases until the level 2, and then it decreases afterwards. In other words, when the open area ratio  $S$  is small, the secondary dominant level exists in the higher level (Case3 levels 1 & 2, Case4 level 2) as well as the substantial space level that is level 0 or 1.

### 3.2. Discussion

It is reasonable that the substantial dominant level is equivalent to the space length of the open area ratio in Table 2 in the image processing result. In order to consider the physical meaning of the secondary dominant level, the image processing result is compared with a previous study. In solid air two phase flow in a pipeline, so-called, inhomogeneous particle density is reported [10]. In the case of large particle size like this study, particles collision becomes the main factor rather than the influence of turbulence as

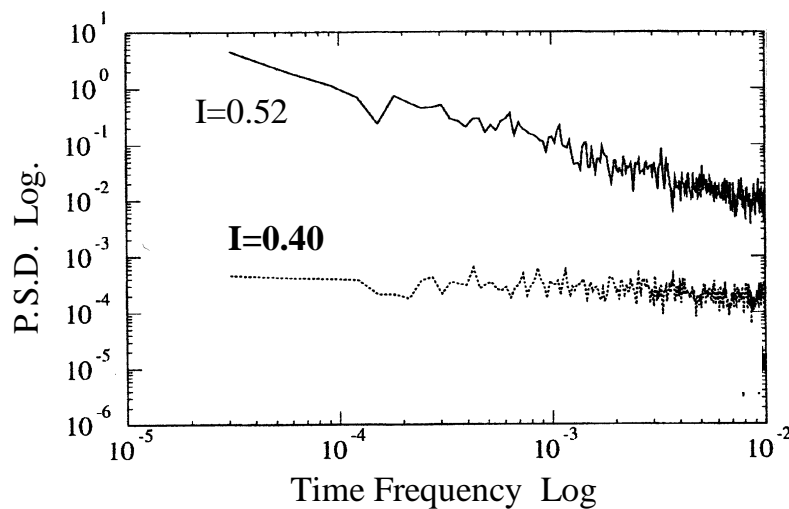


Fig. 6. Fourier spectrum of particle density by LGA G. Peng and H.J. Herrmann [10]

for the inhomogeneous particle density. Peng. [10] calculated the particle density in a cross section of a plumb pipe by lattice gas automaton (LGA) method on the condition that particles fall free from the upper part of the pipe. Figure 6 shows the result of Fourier transform to the calculated particle density on the cross section. When the particle density is low (in the case of particle injection rate  $I = 0.40$ ), the power spectrum density (P.S.D.) maintains the same value. It means the particle density is homogeneous because the collision possibility between particles is low. However, the P.S.D. decreases against the time frequency when the particle density is high (in the case of particle injection rate  $I = 0.52$ ). It means that the particle density gets inhomogeneous because the particles collide each other and to the wall. Namely, in the case of the low open area ratio  $S$  (Cases 3 and 4) in this experiment, the particles pass through the blockage to make the density higher like the case of  $I = 0.52$  of Fig. 6, resulting in the particle collision. Then it is considered that a secondary dominant level occurred due to the inhomogeneous particle density in addition to the substantial space dominant level.

#### 4. Conclusions

Capacitances of particles in a vertical pipeline that installs a blockage are measured to extract the feature image. The followings becomes clear.

- 1) A combination of a capacitance-computed tomography and wavelets transform is useful for extracting a feature of solid-air two-phase flow in a pipeline.
- 2) In the case of low open area ratio of the pipe cross-section, high particle densities are shown in secondary dominant levels as well as a substantial space level. It is realized that the high value in the secondary level resulted from inhomogeneous density due to collision between particles and wall.

#### References

- [1] M. Ochi and M. Takei, Flow Characteristics in Horizontal Pneumatic Conveyance at Low Fluid Velocities, *Advanced Powder Technology* **6**(3) (1996), 317–324.

- [2] M. Takei, M. Ochi, K. Horii, Y.H. Zhao and H. Li, Transporting Particles without Touching Pipe Wall, Forum on Gas-Solid Flows, ASME Summer Annual Meeting Bancouver, Canada, FEDSM97-3629, 1997.
- [3] K. Horii, Y. Matsumae, X. Cheng, M. Takei and B. Hashimoto, An Erosion Resistant Pipe Bend, *Journal of Fluids Engineering ASME* **113**(149) (1991), 149–151.
- [4] K. Hori, T. Fujimoto, K. Kawanishi and H. Nishikawa, 1998, Development of an Ultra-fast X-ray Computed Tomography Scanner System, *Transactions of the Japan Society of Mechanical Engineers* (617) (in Japanese) (1998), 239–244.
- [5] S.M. Huang, A.B. Plaskowski, C.G. Xie and M.S. Beck, Tomographic Imaging of Two-Component Flow Using Capacitance Sensors, *J. Phys. E: Sci. Instrum* **22** (1989), 173–177.
- [6] T. Dyakowski, S.P. Luke, K.L. Ostrowski and R.A. Williams, On-Line Monitoring of Dense Phase Flow Using Real Time Dielectric Imaging, *Powder technol* **104** (1999), 287–295.
- [7] For example, R.K. Young, *Wavelet Theory and its Applications*, Kluwer Academic Publishers, USA, 1993.
- [8] Y. Saito, 1996, Wavelets Analysis for Computational Electromagnetics, *Trans. IEE of Japan* **116A**(10) (in Japanese) (1996), 833–839.
- [9] H. Li, M. Takei, M. Ochi, Y. Saito and K. Horii, Application of Two-dimensional Orthogonal Wavelets to Multiresolution Image Analysis of a Turbulent Jet, *Transactions of the Japan Society for Aeronautical and Space Sciences* **42**(137) (1999), 120–127.
- [10] G. Peng and H.J. Herrmann, Density Waves and 1/f Density Fluctuation in Granular Flow, *Phys. Rev. E* **51**(3) (1995), 1745–1756.